Hindawi
Journal of Sensors
Volume 2022, Article ID 8593750, 15 pages
https://doi.org/10.1155/2022/8593750

Research Article

Wearable BLE Wireless Sensor Based on U-Shaped EBG Monopole Antenna

Minh Thuy Le, Thu Phuong Tran, and Quoc Cuong Nguyen

School of Electrical and Electronic Engineering, Hanoi University of Science and Technology, 10000, Vietnam

Correspondence should be addressed to Quoc Cuong Nguyen; cuong.nguyenquoc@hust.edu.vn

Received 18 March 2022; Revised 16 July 2022; Accepted 18 September 2022; Published 8 October 2022

Academic Editor: Sunil Kumar Singh

In this paper, a compact wearable U-shaped monopole antenna operating at 2.4 GHz frequency band is proposed for Medical Body Area Network applications. The antenna has a compact size of $0.37\lambda \times 0.31\lambda$, covering a band from 2.14 GHz to 3.03 GHz with a gain of 2.3 dBi at 2.45 GHz, and an efficiency of 93% in free space. In addition, an Electromagnetic Band Gap (EBG) metamaterial is utilized to isolate the integrated antenna on the circuit and the body, reducing the Specific Absorption Rate (SAR). In consequence, an integrated circuit employing the EBG ground plane provides a safe value of SAR (0.68 W/kg) when it is attached to a human arm followed by a 74% reduction of SAR value compared to the circuit without EBG (2.57 W/kg). Furthermore, the on-body efficiency of the EBG-based antenna is improved from 54% to 73.68%. Finally, experimental results of a wearable heart rate and blood oxygen level BLE sensor based on the proposed U-shaped EBG monopole antenna exhibit an average power consumption of 108 mW, a sensitivity of -74 dBm, and a maximum Bluetooth Low Energy (BLE) transmission distance with a mobile phone of 16 m in the complex environment.

1. Introduction

Wireless Body Area Network (WBAN) technology has been developed impressively by integrating medical technology and information technology, which presents an application of a sensor network to the human body. However, the integration of antennas on the on-body sensors poses remarkable challenges and difficulties. Indeed, wearable antennas for WBAN applications are required to be compact, efficient, mechanically robust, and easily integrated within a body-worn sensor node. Furthermore, the radiation and impedance characteristics of the antennas should not be affected by the location of the sensors on the body. At the same time, they should be conformal to the body's surface. Various designs have been presented that exhibit desirable characteristics for wearable applications.

Several wideband antennas have been designed for medical devices, which can generally be classified as either dipole/monopole or slot antennas. A dipole antenna operating at 2.4 GHz was studied in [1]. However, this antenna has a relatively large size of $1.46\lambda \times 0.52\lambda$, which increases the difficulty of integration into a wearable device. Monopole antennas are another popular type widely investigated for wearable applications. In [2–4], ultrawideband (UWB) monopole antennas are used for wearable head imaging. Another typical structure is the slot antenna, which helps to create multiple bands [5–10].

Unlike traditional antennas, which are generally positioned in free space, wearable antennas are located near human tissues under various deformation conditions. These tissues have high dielectric constant, affecting antenna's performance such as reflection coefficient (S11), bandwidth, gain, and radiation characteristics. Furthermore, electromagnetic radiation from these antennas needs a Specific Absorption Rate (SAR) level within the health and safety limit set by the European Union (EU) of over 10 g and the United States (US) of over 1 g [11, 12]. To rectify these problems, Electromagnetic Band Gap (EBG) structures were introduced to wearable antennas to provide a high degree of isolation from the human body [13–17]. Metamaterial-based EBG surfaces restrict the propagation of surface waves within a specific frequency band (known as band gap) and therefore reduce the level of unwanted back lobe radiations towards the human body. Hence, when these EBG surfaces

are used as ground planes in the designs of wearable antennas, they limit the value of SAR to the safe level.

Despite notable accomplishments, earlier works only investigated stand-alone antennas and did not integrate them into any circuits while the integration causes a significant impact on the antenna performance. Therefore, this research is dedicated to the following tasks: (1) designing an antenna on the human body and integrating it into the BLE sensor circuit while maintaining a good antenna performance, (2) mounting an EBG layer on the sensor housing to reduce interference and improve circuit efficiency, and (3) creating an on-body BLE sensor with low power consumption.

The paper is organized as follows: Section 2 analyses the on-body antenna in a free space and in the circuit. The performances of this antenna with and without the EBG are presented and discussed in Sections 2 and 3. Section 3.2 presents the proposed on-body BLE wireless sensor performance evaluation in terms of distance of BLE communication and power consumption. The conclusion is in the final section.

2. Design of Wearable BLE Sensors

2.1. U-Shaped Monopole Antenna in a Free Space and on a Body. The U-shaped antenna for wearable applications was designed with the structure as shown in Figure 1. The simulation is carried out in two conditions, free space condition and on human body condition. Antenna operates at Bluetooth frequency band, between 2.4 GHz and 2.483 GHz. The monopole antenna is printed on the 1 mm thickness of FR4 substrate (dielectric constant of 4.3, loss tangent of 0.025) coated with 0.035 mm copper. The antenna parameters are shown in Table 1.

Because the antenna is intended to be used in wearable BLE devices that monitor heart rate and blood oxygen level, a simple model (phantom) of human arm is proposed in this paper. The arm phantom is modelled using CST and it consists of four layers, i.e., skin, fat, muscle, and bone as shown in Figure 2. The materials and design parameters of the arm are the same as described in [15]. The intrinsic properties of each layer are summarized in Table 2. The antenna is placed at 18 mm away from the body to reduce the effect of the body on the antenna performance. This distance will be used to design the bounding box for heart rate and blood oxygen level BLE device.

The simulated S11 and radiation pattern are shown in Figures 3 and 4. When the antenna is in a free space, the S11 is lower than −10 dB between 2.14 GHz and 3.03 GHz (36% bandwidth) with the peak gain of 2.3 dBi and the efficiency of 93%. When the antenna is on the body, the S11 is lower than −10 dB between 2.25 GHz and 2.56 GHz (12.65% bandwidth) with the efficiency of 65.7% and the peak gain of 7.6 dBi because of the human arm. The EBG layer will be designed later to improve antenna efficiency.

2.2. Low-Power BLE Sensor Using a U-Shaped Monopole Integrated Antenna into in a Free Space and on a Body. The BLE technology is well-known for the low-power consumption compared to Zigbee or traditional Bluetooth. With outstanding advantages in terms of energy consumption,

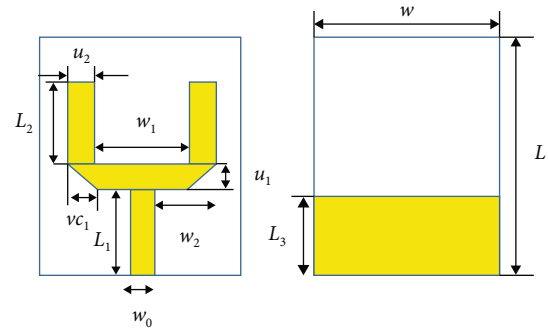

Figure 1: The proposed antenna.

Table 1: Dimension for the antenna.

Parameter	Value (mm)	Parameter	Value (mm)
L	45	w_1	18.5
L_1	15	w_2	10.75
L_2	25.55	u_1	3
L_3	14	u_2	2.5
w	35	vc_1	2.5
w_0	2		

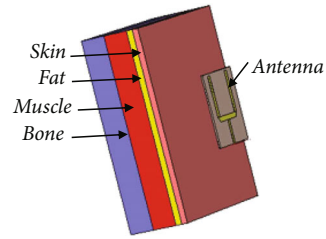

Figure 2: The human arm modelling.

Table 2: Properties of the human arm.

	Skin	Fat	Muscle	Bone
Dielectric constant	38	5.28	52.79	11.38
Conductivity (S/m)	1.46	0.1	1.73	0.39
Density (kg/m^3)	1100	1100	1060	1850
Thickness (mm)	4	4	16	16

MCU DA14585 with fully integrated 2.4 GHz CMOS transceiver which complies with Bluetooth v5.0 is used for the main controller unit of BLE sensor. Figure 5(a) is the block diagram of the BLE sensor. Figure 5(b) is the detailed schematic design of the implementation from the block diagram.

In terms of operating principle, the MCU DA1485 block plays the role of a central microcontroller, processing signals received from the sensor and then transmitted by the antenna block. There are 2 sensor blocks, MAX30100, which measure heart rate and blood oxygen levels based on an infrared method; the second sensor is GY-906 MX90614 and has a noncontact body temperature measurement function, this sensor also based on infrared method. Infrared

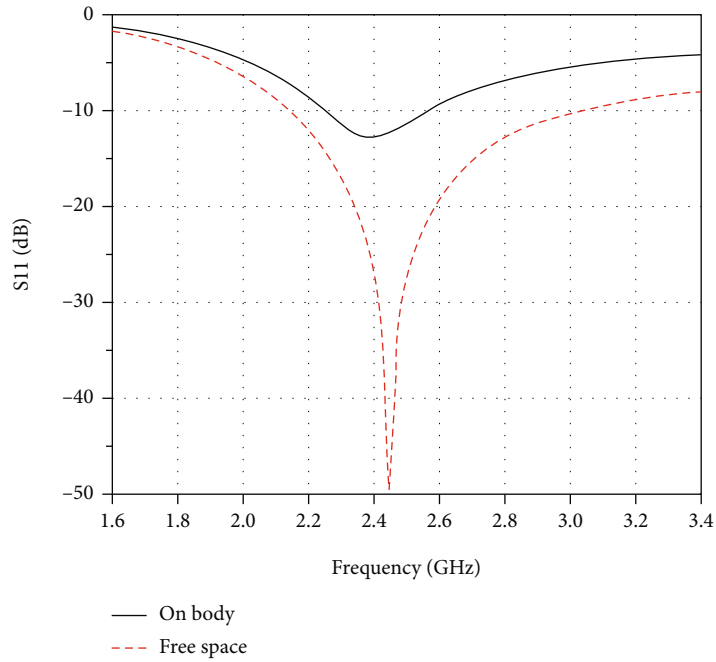

Figure 3: Simulated S11 of the monopole antenna in a free space and 18 mm away from the body.

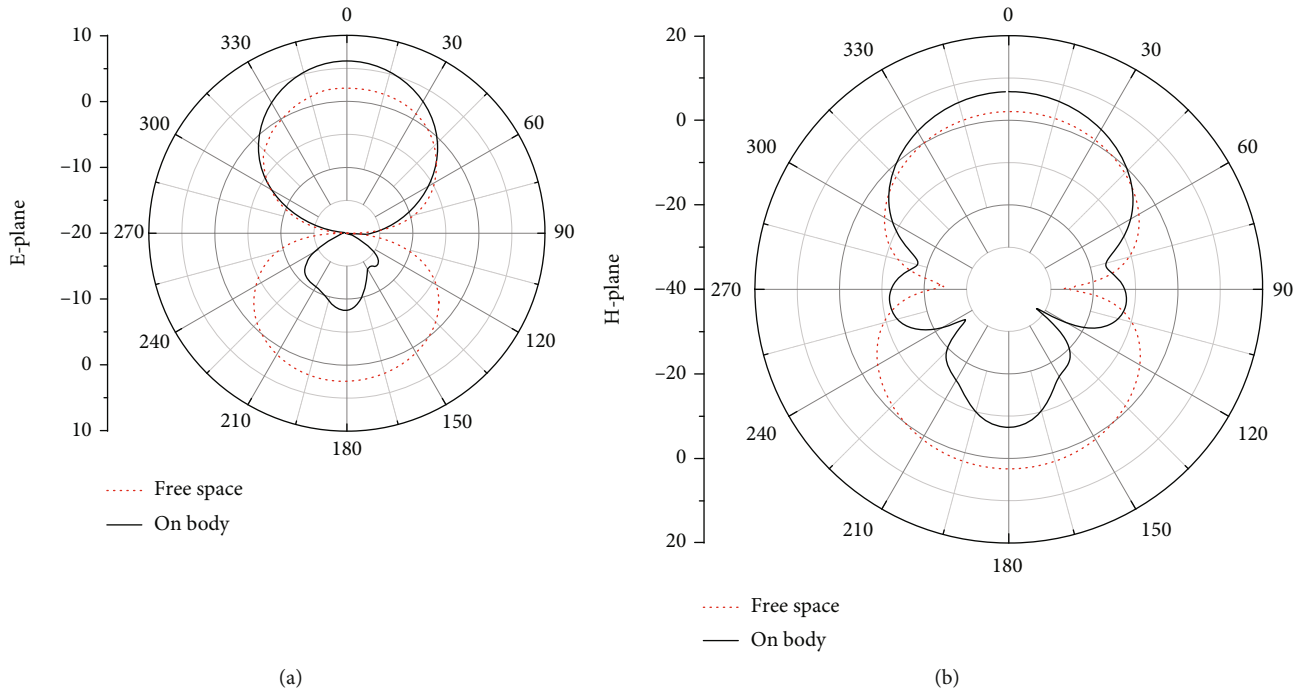

Figure 4: Simulated radiation patterns of the monopole antenna (a) E-plane and (b) H-plane in a free space and 18 mm away from the body.

sensors MLX90614 and MAX30100 are connected to MCU DA14585 through I2C bus. This BLE sensor uses a battery to provide and maintain energy; the battery will provide a voltage of 5 V to the sensors, using an additional voltage stabilizer block to generate a voltage of 3.3 V to supply the central control block. When the BLE transceiver is active, the transmitted and received current of this MCU DA14585 is 3.4 mA and 3.7 mA, respectively. The schematic circuit is presented in Figure 5(b) showing that the U-shaped antenna is connected directly to the RFIO pin 34 of MCU DA14585.

The BLE layout circuit with the integrated antenna is presented in Figure 6. The designed U-shaped antenna in section 2.1 has its ground large enough to insert the BLE sensor layout circuit inside, the coplanar feed of antenna is connected directly to RFIO pin 34 of DA14585 that requires 50 Ω impedance matching at 2.45 GHz. The noncontact

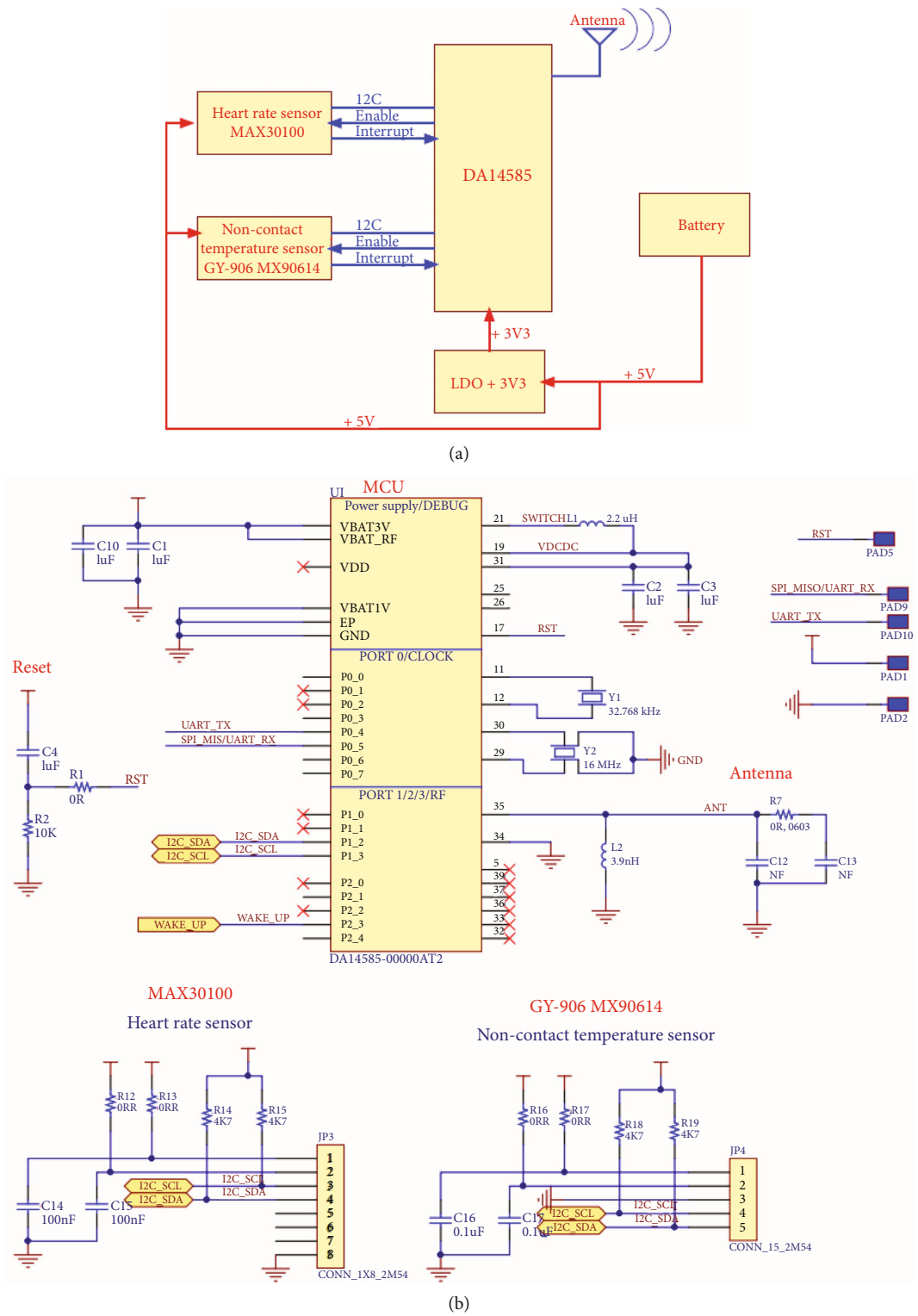

Figure 5: Wearable heart rate and blood oxygen level BLE sensor: (a) function block; (b) schematic.

temperature sensor MLX90614 and the heart rate and blood oxygen level sensor MAX30100 are placed close to the skin and have a small hole on the box at the infrared bulb position of the sensor, allowing the most accurate measurement results. The battery is carefully sealed with the electrodes, insulated from the other components inside. When the BLE circuit is inserted into the ground of the antenna, the antenna is no longer matches its impedance with 50 Ω; it must be changed to shift the resonance frequency to the desired BLE band. The simulated reflection coefficients of U-shaped antenna standing alone and integrated U-shaped antenna BLE sensor in free space are shown in Figure 7(a).

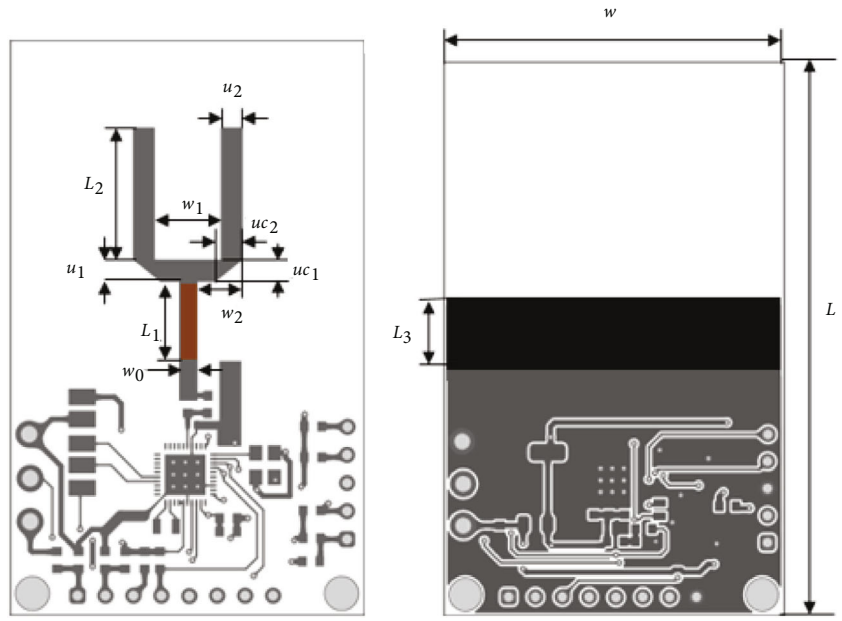

Figure 6: U-shaped monopole antenna integrated into heart rate and blood oxygen level BLE sensor.

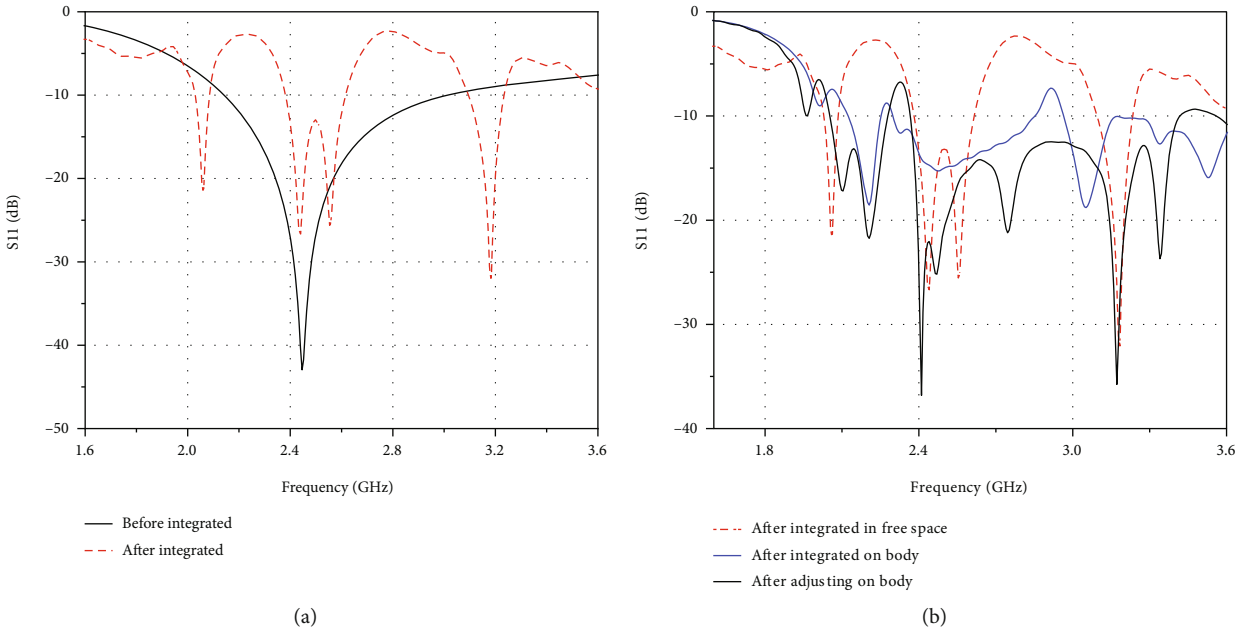

Figure 7: Simulated S11 of (a) U-shaped antenna before integrated and after integrated into BLE sensor in free space and (b) integrated antenna into BLE sensor in free space and on body, before and after adjusting.

After integrating the antenna to the circuit, its size is slightly adjusted to further improve the impedance matching with the circuit board. The reflection coefficient of the adjusted antenna is shown as the black curve in Figure 7(b).

When the BLE sensor is placed on the human arm, due to the impact of the body, the antenna resonant frequency is affected and shifted (long dash-dot red color line in Figure 7(b)). The antenna parameters are adjusted to be well-matched at BLE frequency and are shown as in Figure 7(b), the black color line. This BLE PCB circuit is designed with the size of 52 mm × 32 mm × 1 mm to fit into

Table 3: Dimension of the integrated antenna.

Parameter	Value (mm)	Parameter	Value (mm)
L	52	w_1	6
L_1	7	w_2	4.2
L_2	10	u_1	2
L_3	6	u_2	2
w	32	uc_1	2
w_0	1.6	uc_2	2.5

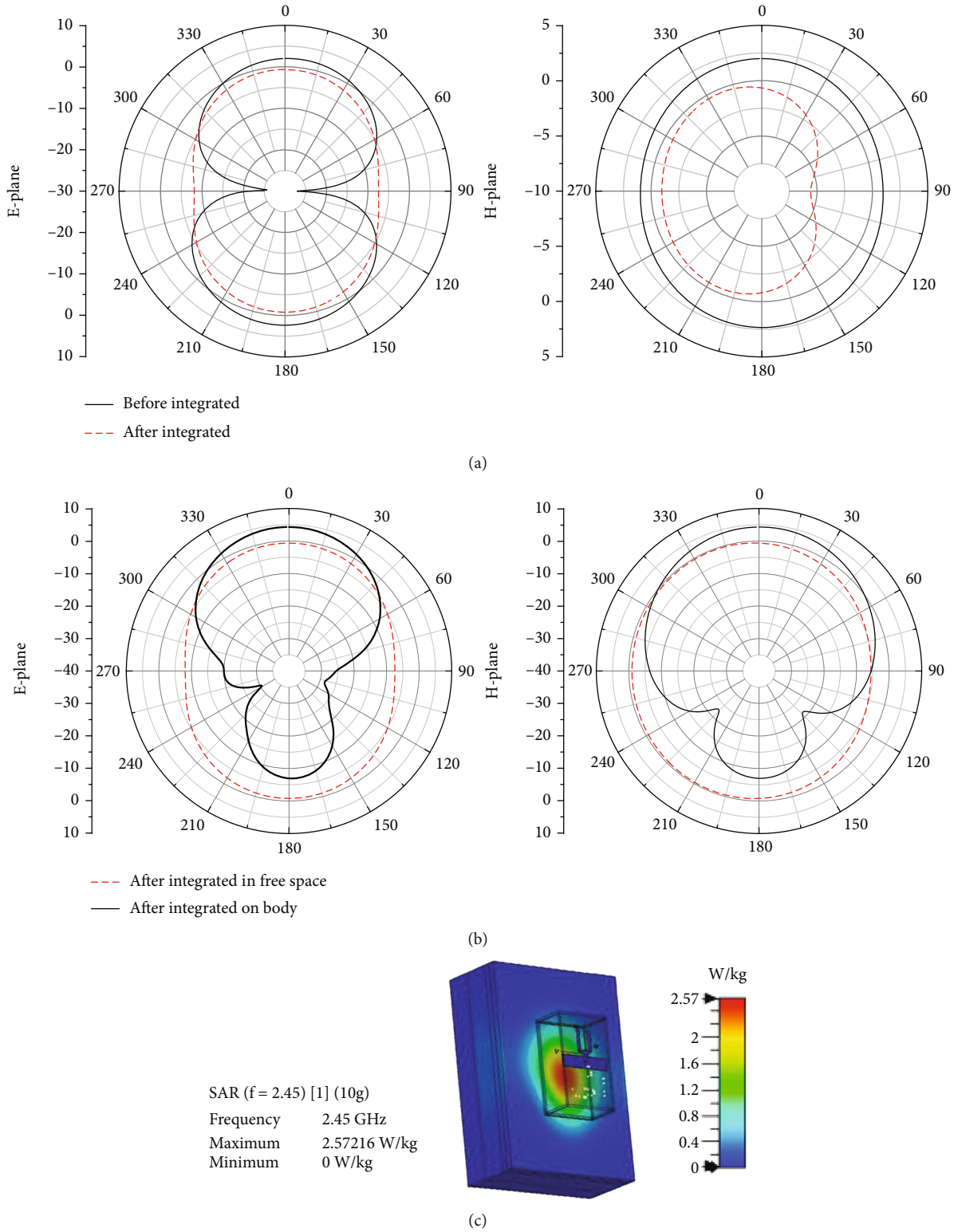

Figure 8: Radiation patterns of (a) the antenna before integrated and after integrated into heart rate and blood oxygen level BLE sensor in free space and (b) integrated antenna into heart rate and blood oxygen level BLE sensor on body before and after adjusting, (c) SAR of integrated antenna on BLE sensor.

the box. The body temperature, heart rate, and blood oxygen level of the human are measured and then transmitted to the monitoring application on the phone via the BLE 5.0 standard.

The resized on-body integrated antenna's parameters are presented in Table 3. The antenna radiation patterns before and after integration into the BLE sensor are illustrated in Figure 8(a). When resized $L_1 = 7\,(\text{mm})$, $L_2 = 10(\text{mm})$, and

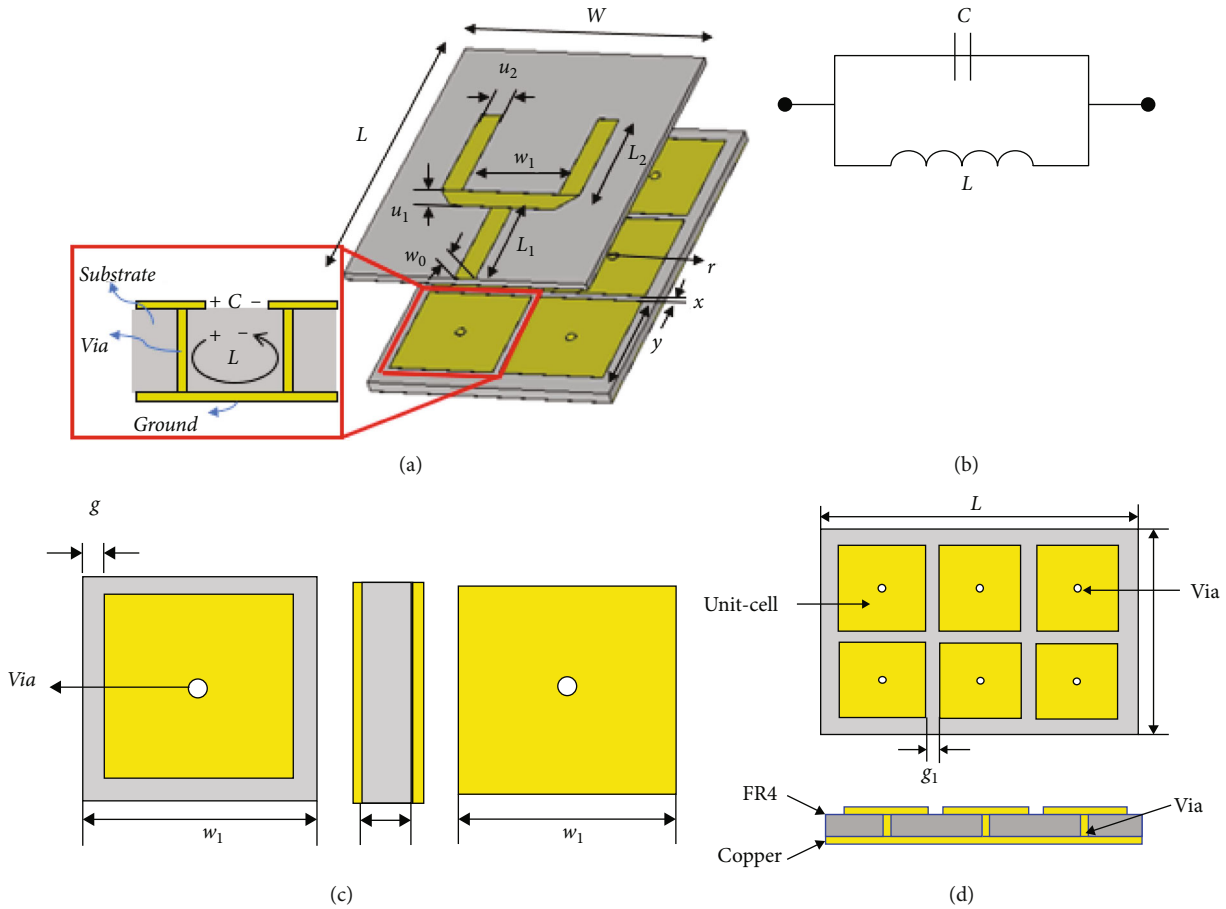

Figure 9: (a) EBG parameters and (b) its equivalent circuit; (c) top view, side view, and front view of an EBG unit-cell; (d) top view and side view of a complete EBG layer.

$w_1 = 6$ (mm), the S11 is lower than -10 dB between 2.36 GHz and 3.42 GHz, corresponding to a bandwidth of 42%, the efficiency is 54.72%, and the peak gain is 5.42 dBi, as shown in Figure 8(b). However, as we can see from Figure 8(c), the value of SAR is 2.57 W/kg, higher than 2 W/kg, exceeding the allowable safety level of body wearable RF devices. Therefore, we place the integrated antenna on the EBG layer to reduce the amount of radiation to the body.

2.3. EBG Design for a Wearable Integrated Antenna. The EBG unit cell structure evolves from a conventional mushroom-like EBG. It consists of a metallic patch and a cylindrical via, passing through the substrate, connecting the patch to the ground of the EBG unit cell as shown in Figure 9.

The operating mechanism of the EBG structure can be explained by an LC filter array or a parallel resonant circuit, as illustrated in Figures 9(a) and 9(b). The inductance is generated by a loop current within the structure through the vias, while the capacitance is generated by the gap of two adjacent patches [18–20].

The values of the capacitance (C), inductance (L), bandwidth (BW), and resonant frequency (f_r) of EBG are given as follows [18–20]:

Table 4: EBG design parameters.

Parameter	Value (mm)	Parameter	Value (mm)
w	32	g_1	1
L	52	h	1.6
w_1	14	Via (radius r)	0.7
g	1.5		

$$L = \mu_0 h, \tag{1}$$

$$C = \frac{W\varepsilon_0(1+\varepsilon_r)}{\pi}\cosh^{-1}\frac{W+g}{g}, \tag{2}$$

$$f_r = \frac{1}{2\pi\sqrt{LC}}, \tag{3}$$

$$\mathrm{BW} = \frac{1}{\eta_0}\sqrt{\frac{L}{C}}, \tag{4}$$

where μ_0, ε_0, and η_0 are the permeability, permittivity, and impedance of free space, respectively, g is the gap between the adjacent patches, and W is the patch width.

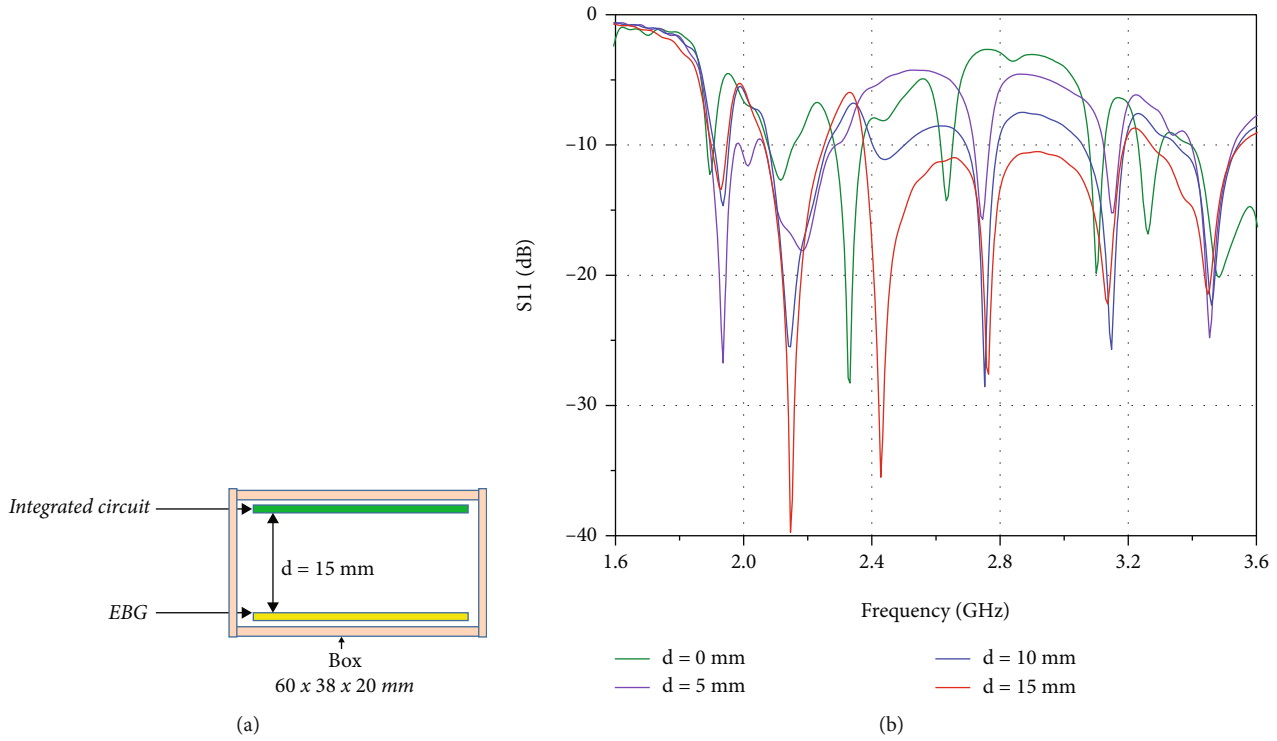

Figure 10: (a) Integrated EBG antenna structure; (b) simulated S11 of integrated antenna with EBG at different distance of d.

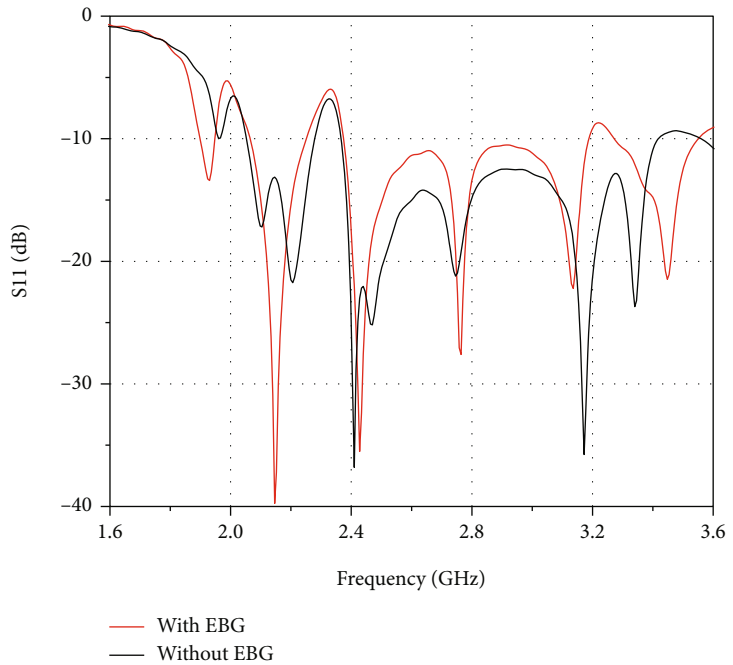

Figure 11: Simulated S11 of integrated antenna on body without EBG and with EBG.

The dimensions of the optimized EBG unit-cell using FR4 substrate with the thickness of 1.6 mm are shown in Table 4.

The integrated antenna is placed above the EBG layer at a distance of d. The reflection coefficient of the integrated antenna changes when d is varied as shown in Figure 10; d = 15 mm is chosen because the S11 is less than -10 dB over a wide band from 2.37 GHz to 3.19 GHz. As the circuit must be small to be placed on the human arm, the EBG layer is designed according to the total size of the BLE sensor's

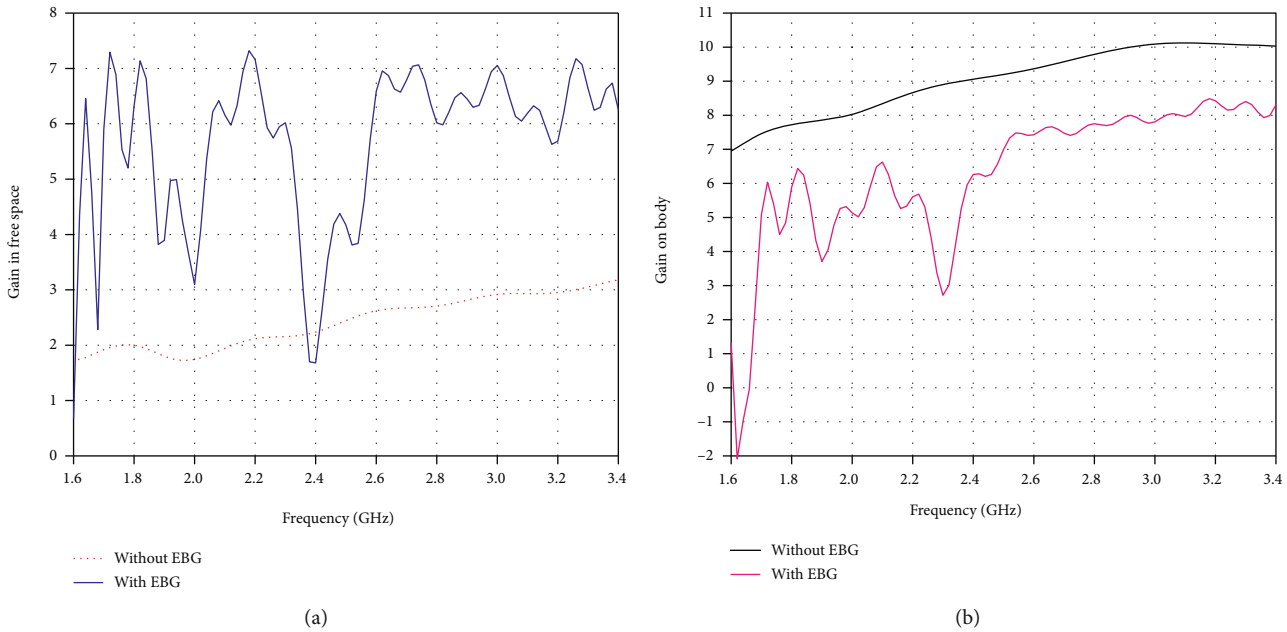

Figure 12: Simulated gain of the antenna in free space (a) and 18 mm away from the body (b).

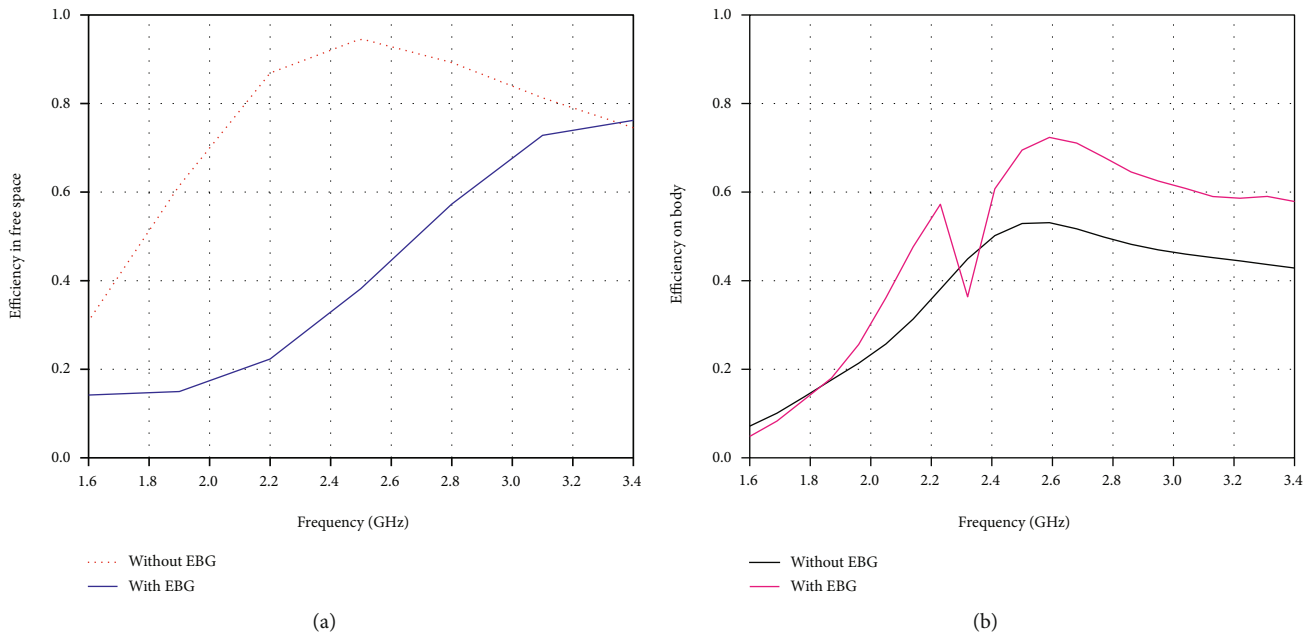

Figure 13: Simulated efficiency of the antenna in free space (a) and 18 mm away from the body (b).

PCB (52 mm × 32 mm) as shown in Figure 9. The EBG layer covers the BLE sensor. We put the integrated circuit in a box with the dimension of 60 mm × 38 mm × 20 mm; the EBG is etched on a face of the box and used as a part of the box to enhance the circuit performance. This complete BLE sensor is small enough to be worn on human arms. The simulated S11, the peak gain, and efficiency versus frequency and radiation pattern of the integrated antenna circuit with EBG on body are shown in Figures 11–14. With the EBG layer, the S11 is lower than -10 dB between 2.37 GHz and 3.19 GHz (33% bandwidth); the efficiency increases from 54.72% to 73.63% while the peak gain increases from 5.42 dBi to 6.87 dBi.

The SAR value of the integrated antenna with EBG is 0.68 W/kg, smaller than 2 W/kg, as shown in Figure 15. With the EBG layer, the BLE sensor meets the required SAR value, within the allowable safe level for wearable RF devices. Besides, the EBG layer can be etched directly on the box of the sensor, as can be seen in the prototype of BLE sensor in Figure 16. The small heart rate and blood oxygen level

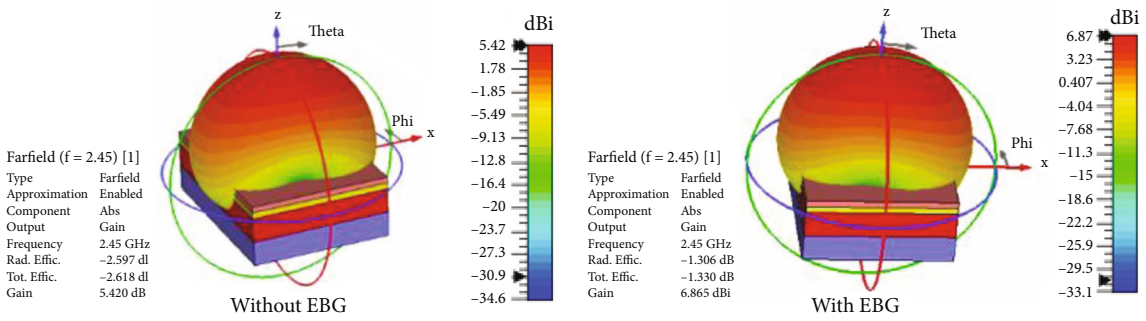

Figure 14: Radiation patterns of the integrated antenna without and with EBG.

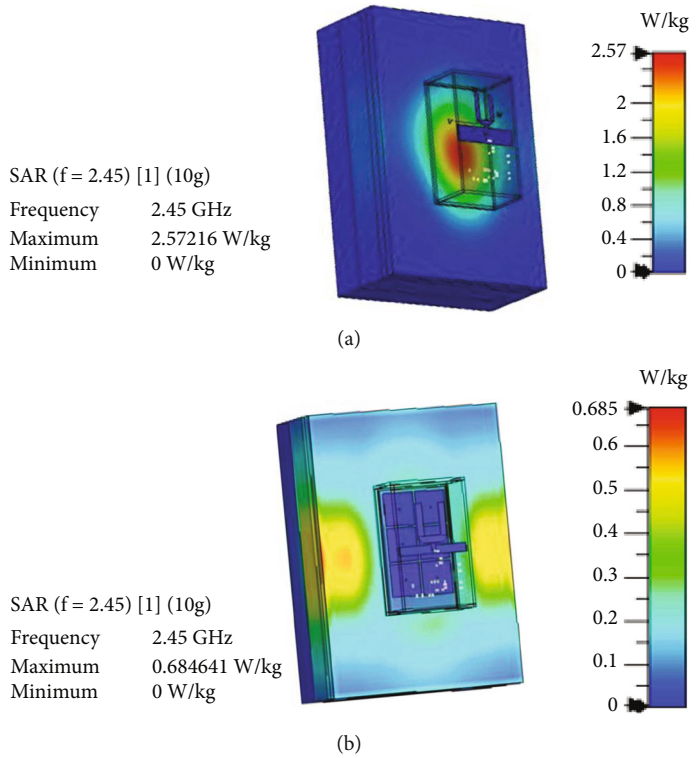

Figure 15: Simulated SAR of integrated antenna on BLE sensor (a) without EBG and (b) with EBG layer.

BLE sensor have potential to be industrialized. Table 5 summarizes all the parameters of integrated antenna on the circuit without and with EBG.

3. Experiment Results

3.1. Integrated Antenna in Wearable BLE Sensor Testing. For an integrated antenna in BLE sensor, it is very difficult to measure and recheck the antenna performance in terms of S11 and radiation pattern as traditional stand-alone antennas because an integrated antenna is excited directly from the RFIO pin of the DA14585 chip and the transmitted power is programmed on the DA14585 chip. Therefore, in this section, we present the measured results of the integrated antenna performances through the read-range and the normalized radiation pattern. The firmware on DA14585 chip is programmed to implement these measurements.

3.1.1. Read-Range Measurement. The read-range measurement configuration for the integrated antenna in the wearable BLE sensor prototype is presented in Figure 17. The wearable BLE sensor (device under test-DUT) is worn on the human arm to transmit BLE signal; one Xiaomi mobile phone is placed on the wood pillar at a distance of R to receive the BLE signal from DUT. The testing scenario is as follows:

(i) Read-range in free space measurement: place the DUT on a wood pillar to transmit BLE signal; vary the distance R between the DUT and the mobile phone to the maximum distance, where the BLE signal can be received; the results are listed in Table 6

(ii) Read-range on body measurement: the DUT is worn on the human arm as Figure 17, moving far away the mobile phone to the maximum distance R, where the

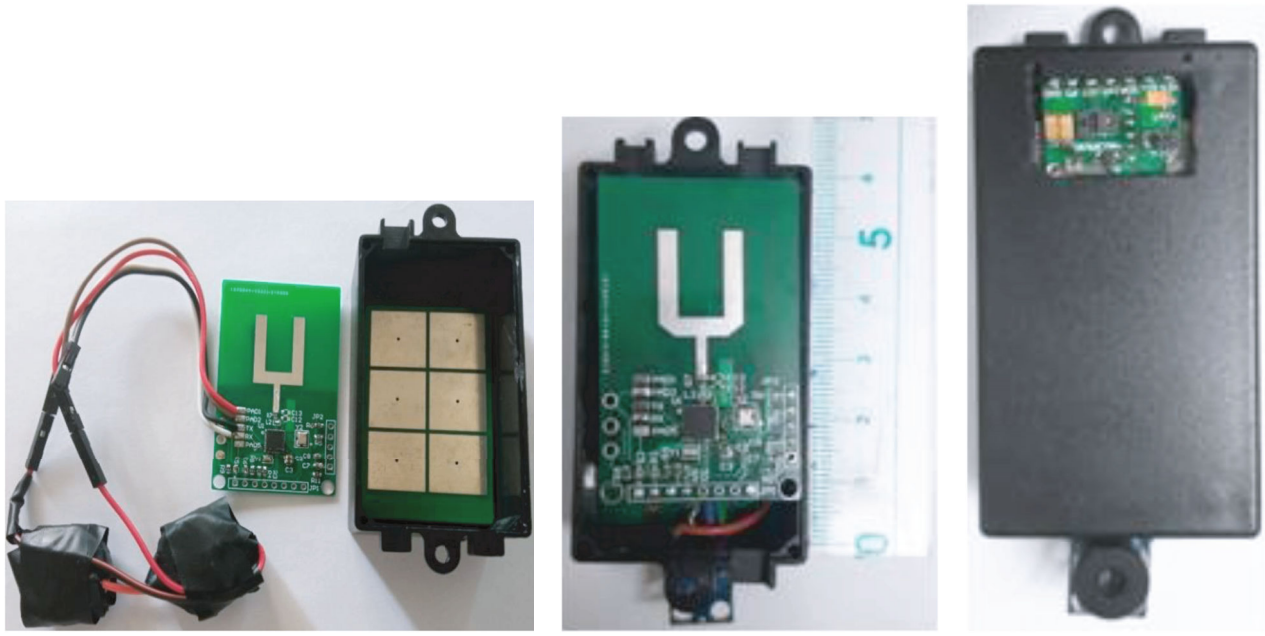

(a) (b) (c)

Figure 16: (a) The heart rate and blood oxygen level BLE sensor: BLE sensor circuit after soldering and the EBG-box; (b) circuit in the box after attaching battery; (c) complete BLE sensor.

Table 5: Summary of integrated circuit without EBG and with EBG results.

Parameter	Without EBG	With EBG
Frequency (GHz)	2.41	2.43
Bandwidth (%)	42.85	33
Gain (dBi)	5.42	6.87
Efficiency (%)	54.74	73.68
SAR_{10g} (W/kg)	2.57	0.68

Table 6: Maximum distance of communication between of BLE sensor and mobile phone.

Test condition		Maximum read-range R (m)
DUT without EBG	In free space	16
	On body	13.5
DUT with EBG	In free space	19
	On body	16

Figure 17: Read-range measurement of U-shaped monopole integrated antenna in wearable BLE sensor.

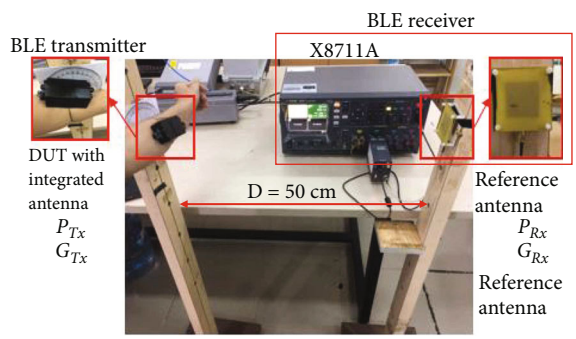

Figure 18: Integrated antenna radiation pattern measurement configuration system using the X8711A test system.

BLE signal can be received; the results are listed in Table 6

3.1.2. Radiation Pattern Measurement. The radiation patterns are important and should be measured to ensure antenna performance. As in Figure 18, wearable BLE sensor (DUT) with integrated antenna operates as a transmitter in the measurement configuration system. The transmitter is represented by the transmitted power P_{Tx} and the antenna gain G_{Tx}. The MCU DA14585 of DUT is programmed to transmit BLE signal with the transmitted power P_{Tx}. The BLE signal then is received by the BLE receiver based on the X8711A system and a reference antenna. The receiver is represented by the received power P_{Rx} and the receiving antenna gain G_{Rx}. The distance between the transmitter

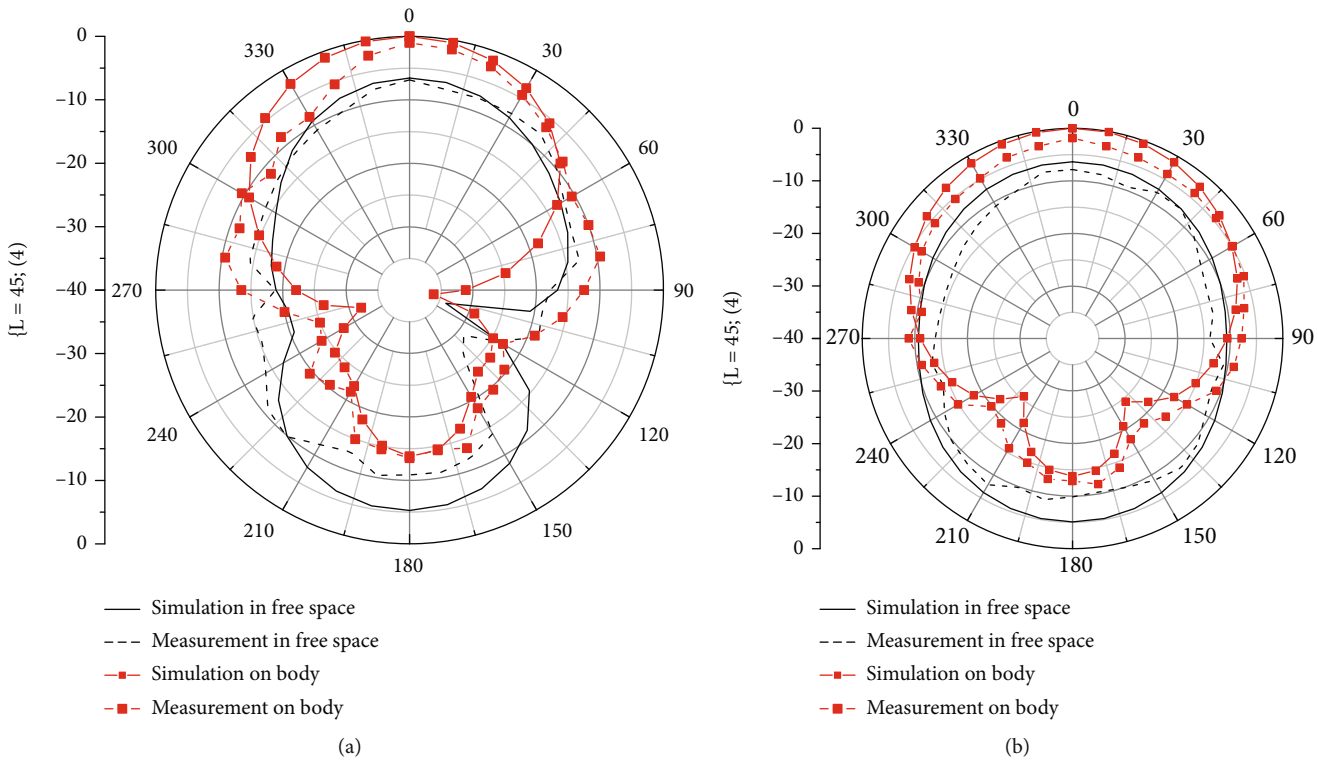

Figure 19: Simulated and measured integrated antenna radiation pattern at 2.45 GHz in free space and on body: (a) E plane; (b) H plane.

and receiver is D. The transmitted antenna gain G_{Tx} is calculated through Friis equation below while P_{Rx}, G_{Rx}, D, λ, and P_{Tx} are known:

$$G_{Rx} = \frac{P_{Rx}}{P_{Tx}G_{Tx}}\left(\frac{4\pi D}{\lambda}\right)^2. \quad (5)$$

The transmitted power is programmed on DA14585 with a fixed value of 0 dBm during this measurement. The DUT is rotated from 0° to 360°; then the BLE receiver measures and displays the received power P_{Rx} by the receiving antenna corresponding with the rotated angle of the BLE transmitter. The DUT antenna gain at each rotated angle is calculated and plotted to illustrate its E plane and H plane. The DUT is placed in the free space and on the arm to measure normalized antenna radiation patterns in the free space and on the body as in Figure 19. The results show that the simulation radiation patterns agree well with the simulation results. There is a small distortion in the measured radiation pattern from 270° to 300° because of the effect of furniture in the room on the received power. However, this difference comes from the complex environment of the room where the measurement has been implemented. The maximum distance of BLE communication is 19 m and 16 m when the DUT is in the free space and on the body, respectively.

Table 7 presents the comparison between the proposed integrated antenna on BLE sensor and the related antennas for medical equipment or IoT devices. The most difficult part of this work is the integration of the antenna on the BLE circuit into the circuit, on the human arm while maintaining its performances. Previous works have designed wearable antennas, but those antennas have not been integrated and placed on the BLE circuit, box, or on human body as this work. The proposed integrated antenna in the BLE sensor is fabricated and tested with an outstanding performance in terms of bandwidth, gain, efficiency, and SAR. As we can see from the table, [9, 24] and this work have the highest efficiency and smallest SAR compared to the related works. However, our antenna gain is higher than the wearable antenna in [9, 24] while antenna efficiency in [24] is higher but its bandwidth is narrower than this work. Although antenna [9] efficiency is higher than this integrated antenna, efficiency of [9] will be reduced when it is integrated and tested into circuit.

3.2. BLE Sensor: Testing and Evaluation. It is important to validate the receiver sensitivity and power consumption of a BLE sensor. Receiver sensitivity is the minimum BLE signal that the receiver can decode with a packet error rate (PER) = 0%. This sensitivity of -74 dBm is measured using the X8711A IoT measurement system of Keysight, as in Figure 20; it is passing the BLE standard requirement (-70 dBm) according to [26].

The power consumption of the proposed BLE sensor is determined through an IoT measurement system with the results listed in Table 8. The average current consumption of the BLE sensor before adding sensors and after adding the sensors is 3.17 mA and 32.68 mA, respectively, and the power consumption of the whole circuit before and after adding the sensors when transmitting is 25.67 mW and 487.83 mW, respectively. Before installing the sensor on the

Table 7: Comparison of the proposed antenna on body with some references.

Ref.	Size (λ_g)	BW (%)	Gain (dBi)	Eff. (%)	SAR_{10} (W/kg)/P_{input} (W)
[1]	1.46×0.52	14	—	—	2.25 -
[5]	$0.18 \times 0.18 \times 0.04$	14.1	0.919	—	0.1 -
[9]	$0.2 \times 0.29 \times 0.009$	33.3	2.18	81.4	<2 0.265
[10]	$0.32 \times 0.32 \times 0.004$	7.9	2.06	45	-0.34
[15]	$0.68 \times 0.48 \times 0.02$	5	7.3	70	—
[16]	$0.68 \times 0.48 \times 0.02$	8.3	6.55	—	5.99 1
[17]	$0.68 \times 0.48 \times 0.02$	14.7	7.3	70	0.23 -
[21]	$0.36 \times 0.26 \times 0.014$	144	6.57	96.99	—
[22]	$0.58 \times 0.42 \times 0.03$	85.4	5.65	99.35	—
[23]	$1.08 \times 0.67 \times 0.04$	120	7.46	99.3	—
[24]	0.437×0.025	22.9	3.5	95	0.191 -
[25]	0.64×0.16	5.2	2.71	—	0.0091 -
This work	$0.86 \times 0.53 \times 0.01$	33	6.87	73.68	0.68 0.5

λ_g is the wavelength in the dielectric at 2.4 GHz; BW means bandwidth.

(a)

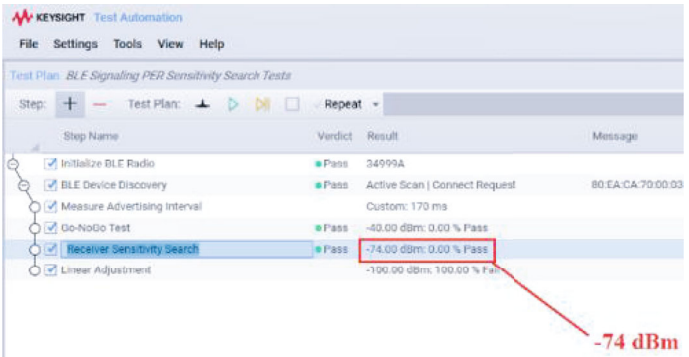

(b)

Figure 20: (a) Receiver sensitivity and power consumption of BLE sensor using Keysight's X8711A IoT measurement system. (b) Receiver sensitivity result on the tool.

Table 8: Power consumption of the circuit before and after the sensor is added.

		Current consumption (max.) (mA)	Average current (mA)	Voltage (V)	Power consumption (mW)	Lifetime of the circuit when measuring and transmitting every 1 s (h)
Before adding the sensor	Current max (mA)	7.78	3.17	3.3	25.67	287
	Current min (mA)	2.5		3.3	8.25	
After adding the sensor	Current max (mA)	147.83	32.68	3.3	487.83	27
	Current min (mA)	8		3.3	26.4	

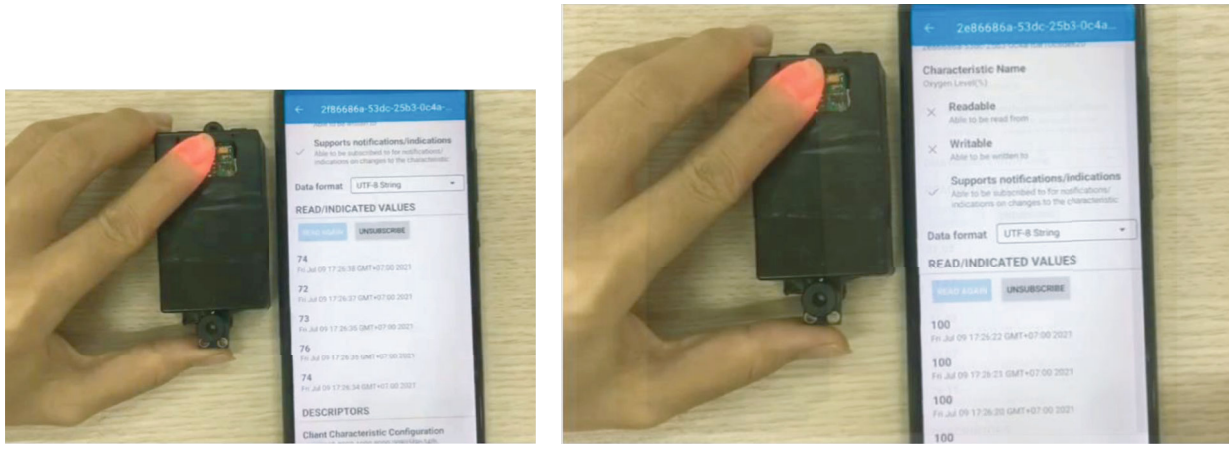

(a) (b)

Figure 21: Wearable BLE sensor testing on a normal human (a) heart rate and (b) blood oxygen level.

BLE circuit, the minimum and maximum power consumption of the BLE circuit during active mode, transmitting, and receiving modes with a period of 1 s is 8.25 mW and 25.67 mW, respectively. After adding the sensors, its minimum and maximum power consumption is 26.4 mW and 487.83 mW, respectively. We can then calculate the BLE sensor lifetime in the case it transmits BLE with a data transmission cycle of 1 s using 4-coin batteries (220 mAh) as a power supply for the BLE device. The lifetime of the BLE circuit is 287 h without sensors and 27 h with sensors correspondingly.

The wearable BLE sensor is tested to measure the body temperature, heart rate, and blood oxygen level and is presented in Figure 21. For a normal human, the blood oxygen level is 100 with a heart rate of 74 and body temperature of 33°.

4. Conclusions

In this paper, a wearable antenna is designed, analyzed, and integrated on a circuit. The integrated antenna is placed on the body with a bandwidth of 42%, a gain of 5.42 dBi, an efficiency of 54.72%, and SAR of 2.57 W/kg > 2 W/kg. The metamaterial surface has been applied as an EBG layer embedded into the circuit box, the antenna efficiency is increased from 54.74% to 73.63%, while its SAR value of 0.68 W/kg < 2 W/kg is achieved when using the EBG layer. The proposed BLE sensor is tested and evaluated with a good BLE transmission and reception up to 19 m. The proposed BLE circuit has passed the BLE sensitivity standard, and from that, we can calculate the number of hours of using the circuit until the battery runs out.

Data Availability

The data used to support the findings of this study are included within the article.

Conflicts of Interest

The authors declare that there are no conflicts of interest regarding the publication of this paper.

Acknowledgments

The authors wish to thank all members of RF3I lab for their help during our measurement and experimentations. This research is funded by Hanoi University of Science and Technology under grant number T2021-SAHEP-007.

References

[1] N. A. Elias, N. A. Samsuri, M. K. A. Rahim, and N. Othman, "The effects of human body and bending on dipole textile antenna performance and SAR," in *2012 Asia Pacific Microwave Conference Proceedings*, pp. 34–36, Kaohsiung, Taiwan, 2012.

[2] M. S. Bashri, T. Arslan, and W. Zhou, "Flexible antenna array for wearable head imaging system," in *2017 11th European Conference on Antennas and Propagation (EUCAP)*, pp. 172–176, Paris, France, 2017.

[3] C. Andreu, C. Garcia-Pardo, A. Fomes-Leal, M. Cabedo-Fabres, and N. Cardona, "UWB in-body channel performance by using a direct antenna designing procedure," in *2017 11th European Conference on Antennas and Propagation (EUCAP)*, pp. 278–282, Paris, France, 2017.

[4] H. A. Elmobarak Elobaid, S. K. Abdul Rahim, M. Himdi, X. Castel, and M. Abedian Kasgari, "A transparent and flexible polymer-fabric tissue UWB antenna for future wireless networks," *IEEE Antennas and Wireless Propagation Letters*, vol. 16, pp. 1333–1336, 2017.

[5] A. Kumar and R. K. Badhai, "A dual-band on-body printed monopole antenna for body area network," in *2017 International Conference on Inventive Systems and Control (ICISC)*, pp. 1–5, Coimbatore, India, 2017.

[6] S. R. Zahran, A. Gaafar, and M. A. Abdalla, "A flexible UWB low profile antenna for wearable applications," in *2016 IEEE International Symposium on Antennas and Propagation (APSURSI)*, pp. 1931-1932, Fajardo, PR, USA, 2016.

[7] B. Yeboah-Akowuah, P. Kosmas, and Y. Chen, "A Q-slot monopole for UWB body-centric wireless communications," *IEEE Transactions on Antennas and Propagation*, vol. 65, no. 10, pp. 5069–5075, 2017.

[8] H. F. Abutarboush, W. Li, and A. Shamim, "Flexible-screen-printed antenna with enhanced bandwidth by employing defected ground structure," *IEEE Antennas and Wireless Propagation Letters*, vol. 19, no. 10, pp. 1803–1807, 2020.

[9] A. Smida, A. Iqbal, A. J. Alazemi, M. I. Waly, R. Ghayoula, and S. Kim, "Wideband wearable antenna for biomedical telemetry applications," *IEEE Access*, vol. 8, pp. 15687–15694, 2020.

[10] A. Arif, M. Zubair, M. Ali, M. U. Khan, and M. Q. Mehmood, "A compact, low-profile fractal antenna for wearable on-body WBAN applications," *IEEE Antennas and Wireless Propagation Letters*, vol. 18, no. 5, pp. 981–985, 2019.

[11] U. Ali, S. Ullah, J. Khan et al., "Design and SAR analysis of wearable antenna on various parts of human body, using conventional and artificial ground planes," *Journal of Electrical Engineering and Technology*, vol. 12, no. 1, pp. 317–328, 2017.

[12] A. Y. I. Ashyap, S. H. B. Dahlan, Z. Z. Abidin et al., "Robust and efficient integrated antenna with EBG-DGS enabled wide bandwidth for wearable medical device applications," *IEEE Access*, vol. 8, pp. 56346–56358, 2020.

[13] A. Y. Ashap, Z. Z. Abidin, S. H. Dahlan et al., "Flexible wearable antenna on electromagnetic band gap using PDMS substrate," *TELKOMNIKA (Telecommunication Computing Electronics and Control)*, vol. 15, pp. 1454–1460, 2017.

[14] P. Sambandam, M. Kanagasabai, S. Ramadoss et al., "Compact monopole antenna backed with fork-slotted EBG for wearable applications," *IEEE Antennas and Wireless Propagation Letters*, vol. 19, no. 2, pp. 228–232, 2020.

[15] M. A. Antoniades, M. A. B. Abbasi, M. Nikolic, P. Vryonides, and S. Nikolaou, "Conformai wearable monopole antenna backed by a compact EBG structure for body area networks," in *2017 11th European Conference on Antennas and Propagation (EUCAP)*, pp. 164–166, Paris, France, 2017.

[16] H. S. Vu, N. Nguyen, N. Ha-Van, C. Seo, and M. T. Le, "Multiband ambient RF energy harvesting for autonomous IoT devices," *IEEE Microwave and Wireless Components Letters*, vol. 30, no. 12, pp. 1189–1192, 2020.

[17] G.-P. Gao, B. Hu, S.-F. Wang, and C. Yang, "Wearable circular ring slot antenna with EBG structure for wireless body area network," *IEEE Antennas and Wireless Propagation Letters*, vol. 17, no. 3, pp. 434–437, 2018.

[18] D. Sievenpiper, Z. Lijun, R. F. J. Broas, N. G. Alexopolous, and E. Yablonovitch, "High-impedance electromagnetic surfaces with a forbidden frequency band," *IEEE Transactions on Microwave Theory and techniques*, vol. 47, no. 11, pp. 2059–2074, 1999.

[19] F. Yang and Y. Rahmat-Samii, *Electromagnetic Band Gap Structures in Antenna Engineering*, Cambridge University Press, Cambridge, 2008.

[20] A. Y. I. Ashyap, S. H. B. Dahlan, Z. Zainal Abidin et al., "An overview of electromagnetic band-gap integrated wearable antennas," *IEEE Access*, vol. 8, pp. 7641–7658, 2020.

[21] A. De, B. Roy, A. Bhattacharya, and A. K. Bhattacharjee, "Bandwidth-enhanced ultra-wide band wearable textile antenna for various WBAN and Internet of Things (IoT) applications," *Radio Science*, vol. 56, 2021.

[22] A. De, B. Roy, and A. K. Bhattacharjee, "Dual-notched monopole antenna using DGS for WLAN and Wi-MAX applications," *Journal of Circuits, Systems and Computers*, vol. 28, article 1950189, 2019.

[23] A. De, B. Roy, A. Bhattacharya, and A. K. Bhattacharjee, "Investigations on a circular UWB antenna with Archimedean spiral slot for WLAN/Wi-MAX and satellite X-band filtering feature," *International Journal of Microwave and Wireless Technologies*, vol. 14, pp. 781–789, 2022.

[24] T. Govindan, S. K. Palaniswamy, M. Kanagasabai, S. Kumar, T. R. Rao, and M. G. N. Alsath, "Conformal quad-port UWB MIMO antenna for body-worn applications," *International Journal of Antennas and Propagation*, vol. 2021, Article ID 9409785, 13 pages, 2021.

[25] F. R. Kareem, M. El Atrash, A. A. Ibrahim, and M. A. Abdalla, "All-textile inspired-folded dipole antennas for on/off-body communications medical applications," *Alexandria Engineering Journal*, vol. 61, pp. 8751–8761, 2022.

[26] Bluetooth SIG, *Bluetooth Core Specification V5.2*, 2019.